Pulses of Ca^{2+} coordinate actin assembly and exocytosis for stepwise cell extension

Norio Takeshita[a,b,1], Minoas Evangelinos[a,c], Lu Zhou[d,e], Tomoko Serizawa[b], Rosa A. Somera-Fajardo[a], Ling Lu[f], Naoki Takaya[b], G. Ulrich Nienhaus[d,e,g,h], and Reinhard Fischer[a]

[a]Department of Microbiology, Institute for Applied Bioscience, Karlsruhe Institute of Technology, 76131 Karlsruhe, Germany; [b]Faculty of Life and Environmental Sciences, University of Tsukuba, Tsukuba 305-8572, Japan; [c]Faculty of Biology, University of Athens, Athens 15784, Greece; [d]Institute of Applied Physics, Karlsruhe Institute of Technology, 76131 Karlsruhe, Germany; [e]Institute of Nanotechnology, Karlsruhe Institute of Technology, 76344 Eggenstein-Leopoldshafen, Germany; [f]College of Life Sciences, Nanjing Normal University, 210023 Nanjing, China; [g]Department of Physics, University of Illinois at Urbana–Champaign, Urbana, IL 61801; and [h]Institute of Toxicology and Genetics, Karlsruhe Institute of Technology, 76344 Eggenstein-Leopoldshafen, Germany

Edited by Jay C. Dunlap, Geisel School of Medicine at Dartmouth, Hanover, NH, and approved April 13, 2017 (received for review January 6, 2017)

Many eukaryotic cells grow by extending their cell periphery in pulses. The molecular mechanisms underlying this process are not yet fully understood. Here we present a comprehensive model of stepwise cell extension by using the unique tip growth system of filamentous fungi. Live-cell imaging analysis, including superresolution microscopy, revealed that the fungus *Aspergillus nidulans* extends the hyphal tip in an oscillatory manner. The amount of F-actin and secretory vesicles (SV) accumulating at the hyphal tip oscillated with a positive temporal correlation, whereas vesicle amounts were negatively correlated to the growth rate. The intracellular Ca^{2+} level also pulsed with a positive temporal correlation to the amount of F-actin and SV at the hyphal tip. Two Ca^{2+} channels, MidA and CchA, were needed for proper tip growth and the oscillations of actin polymerization, exocytosis, and the growth rate. The data indicate a model in which transient Ca^{2+} pluses cause depolymerization of F-actin at the cortex and promote SV fusion with the plasma membrane, thereby extending the cell tip. Over time, Ca^{2+} diffuses away and F-actin and SV accumulate again at the hyphal tip. Our data provide evidence that temporally controlled actin polymerization and exocytosis are coordinated by pulsed Ca^{2+} influx, resulting in stepwise cell extension.

oscillation | calcium | actin | *Aspergillus* | filamentous fungi

Cells extend their periphery before division and thereby maintain their original size and shape. Spatial and temporal observations have shown that cell extension does not occur continuously but stepwise. This phenomenon is shared by fission yeast (1), filamentous fungi (2), mammalian polarized neurons (3), nonpolarized cells (4), plant root hairs (5), and pollen tubes (6). Stepwise cell extension is driven by oscillations in the supply of proteins and lipids mediated by vesicle trafficking and cytoskeleton dynamics. Intracellular Ca^{2+} levels regulate actin assembly and vesicle fusion (7, 8). The Ca^{2+} level also oscillates and, consequently, could be closely related with stepwise cell extension (4–6). The molecular mechanism underlying discontinuous cell extension, however, has remained elusive.

Filamentous fungi grow as highly polarized tubular cells that indefinitely extend the cell body at one end in a process called "tip growth." During tip growth the cell-extension site is maintained at the hyphal tip, where accumulation of F-actin, active exocytosis, and growth rate can be monitored simultaneously. Thus, filamentous fungi are excellent systems for the analysis of stepwise cell extension and the understanding of cell-shape determination (9–11). The extension of hyphal tips requires constant enlargement of the cell membrane. The supply of proteins and lipids is achieved by vesicle trafficking via the actin and microtubule cytoskeletons with their corresponding motor proteins (12–16). Microtubules serve as tracks of secretory vesicles (SV) for long-distance transport to the hyphal tip and are important for rapid hyphal growth (17). Actin cables, formed from the hyphal tip in retrograde direction, are involved in exocytosis and SV accumulation before exocytosis (18, 19). Vesicle accumulation before secretion results in the formation of a fungal-specific structure, called the Spitzenkörper (20). Besides these fungal-specific microstructures, most constituents of the fungal-tip growth apparatus are shared with other eukaryotic cells that extend in a stepwise fashion. Hence, filamentous fungi are great models for studying the mechanism of oscillatory growth.

Stepwise cell extension at hyphal tips was reported in several filamentous fungi 20 y ago (2); still, only a few details on the molecular mechanism have been revealed since. Our recent study using superresolution fluorescence microscopy revealed that the membrane-associated polarity marker, TeaR (21), transiently assembles at the hyphal tip membrane of *Aspergillus nidulans* and disperses along the membrane after exocytosis, which inserts a new membrane and results in local membrane extension (22). This observation suggested a "transient polarity assembly model," which explains that fungal-tip cells extend by a repetition of coordinated steps, assembly/disassembly of TeaR, actin polymerization, and exocytosis, rather than by constant elongation (22, 23). Oscillations of the Ca^{2+} level have been observed at hyphal tips in filamentous fungi (24). These observations strongly suggest that stepwise extension of hyphal tips requires the concerted action of Ca^{2+}, actin, and exocytosis.

Significance

The day–night rhythm in living organisms controls many processes, which then oscillate in a circadian manner. In addition, there are many processes that appear continuous but the underlying mechanisms oscillate with distinct periods. For example, eukaryotic cells grow by extending their cell periphery in pulses rather than by continuous extension. Here we investigate the molecular basis for such oscillatory growth by using the unique tip growth system of filamentous fungi, where actin assembly, exocytosis, and growth rate were observed simultaneously. We provide evidence that temporally controlled actin assembly and exocytosis are coordinated by pulsed Ca^{2+} influxes, resulting in stepwise cell extension. This mechanism allows the cells to respond more quickly to both internal and environmental cues, including chemical and mechanical stimuli.

Author contributions: N. Takeshita and R.F. designed research; N. Takeshita, M.E., L.Z., and T.S. performed research; L.Z., R.A.S.-F., L.L., and G.U.N. contributed new reagents/analytic tools; N. Takeshita and L.Z. analyzed data; and N. Takeshita, N. Takaya, G.U.N., and R.F. wrote the paper.

The authors declare no conflict of interest.

This article is a PNAS Direct Submission.

[1]To whom correspondence should be addressed. Email: takeshita.norio.gf@u.tsukuba.ac.jp.

This article contains supporting information online at www.pnas.org/lookup/suppl/doi:10.1073/pnas.1700204114/-/DCSupplemental.

Here we demonstrate critical correlations between the intracellular Ca^{2+} level, actin polymerization, exocytosis, and cell extension at fungal tips, and provide evidence that temporally controlled actin polymerization and exocytosis drive stepwise cell extension, which are coordinated by pulsed Ca^{2+} influx. Because the switch from yeast to the hyphal growth form is often a pathogenicity factor in animal and plant pathogens, and the hyphal secretion machinery is also required for the production of commercial enzymes and reagents, understanding the tip-growth machinery may impact medical and agricultural antifungal agent development and the improvement of fungi as valuable biotechnological work horses (25–27).

Results

Oscillation of the Fungal-Tip Cell-Extension Rate. We investigated the cell-extension rate of hyphae in *A. nidulans* for 30 min in 10-s intervals (Fig. 1*A* and Movie S1). The average cell-extension rate of 1.8 μm/min (0.03 μm/s) was derived from a kymograph along the growth axis (Fig. 1*B*). When the extension distance of the tip position was measured every 20 s (Fig. 1*C*), a line graph showed unevenness and fluctuation of the distance from 0.4 to 1 μm in 20 s, indicating pulsed growth of the hyphae (Fig. S1*A*). Because the dynamics was not reliably measurable as a result of the limited spatial resolution of conventional light microscopy, we applied superresolution photoactivation localization microscopy (PALM) (28, 29). We imaged hyphae producing a fusion protein of chitin synthase class III (ChsB), which localizes at the plasma membrane and is transported by the SV (30), and mEosFP*thermo* using wide-field fluorescence microscopy (31). mEosFP*thermo*, a thermostable, monomeric variant of the green-to-red photoconverting fluorescent protein, EosFP (32, 33), is widely used for conventional fluorescence imaging. The PALM images showed ChsB clusters at the apical membrane. We applied a "moving-window binning" technique to generate sequences of PALM images in 20-s intervals for a total duration of 140 s (Fig. 1*D*) (22). The temporal changes of the apical cell edges were compared in 20-s intervals (Fig. 1*E*). Larger extensions of the apical membrane were occasionally observed from 40 to 60 s, from 100 to 120 s, and from 120 to 140 s (Fig. 1*E* and Fig. S1*B*). These results revealed that the cell-extension rate of hyphae is not constant but varies in an oscillatory manner.

Next, we asked whether polymerization of actin and the amount of SV at the hyphal tips correlate with the oscillation of the cell-extension rate. F-actin and SV were visualized by fluorescence of GFP-tagged tropomyosin (TpmA) and mCherry-tagged ChsB, respectively (18, 30). Prominent signals were visible at the hyphal

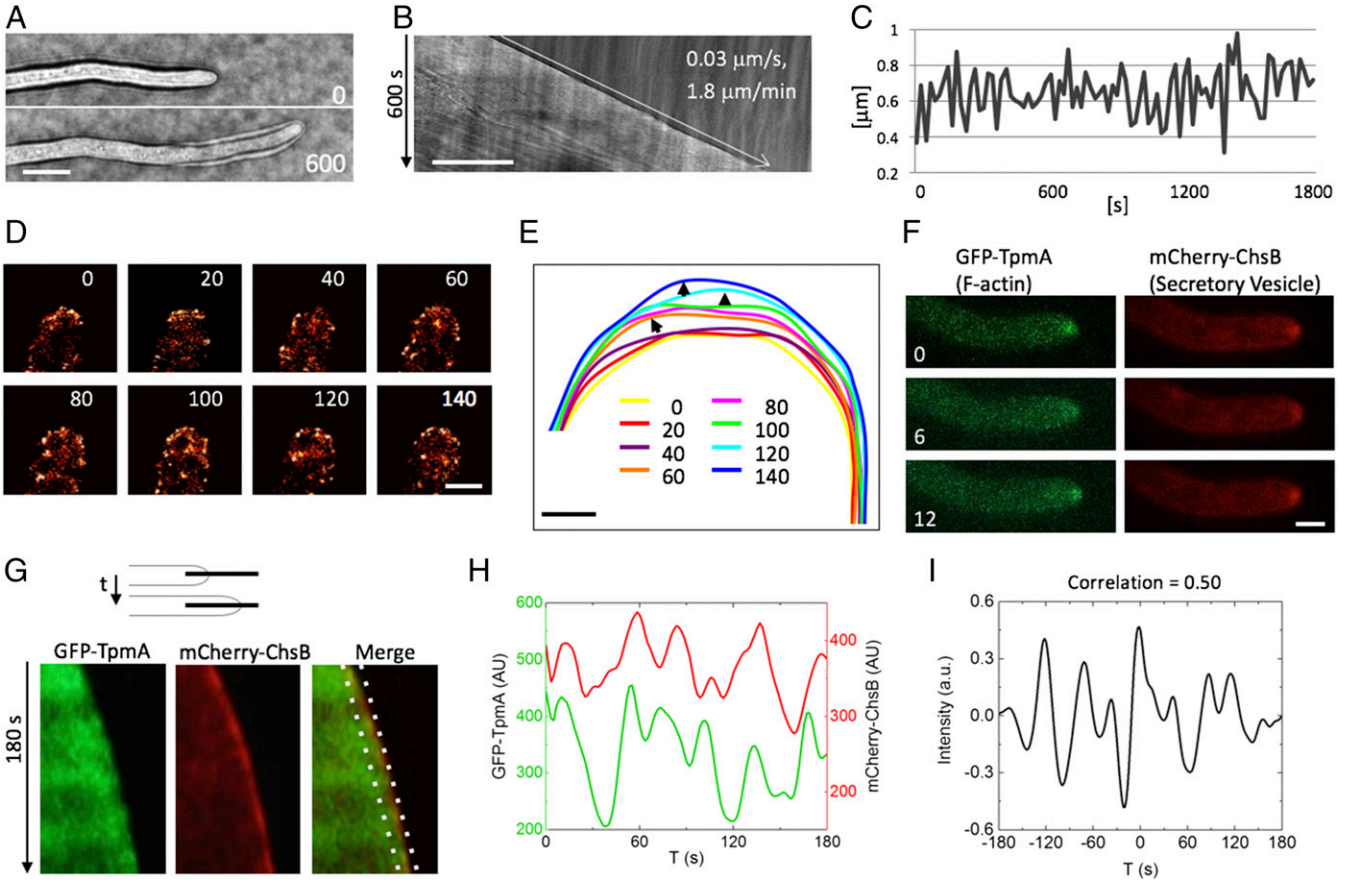

Fig. 1. Stepwise growth of hyphae. (*A*) DIC images of growing hyphae. Wild-type *A. nidulans* was grown in minimal media at room temperature. The elapsed time is given in seconds. (Scale bar, 10 μm.) (*B*) Kymograph of the growing hypha in *A* along the growth axis. Total 600 s. (Scale bar, 5 μm.) (*C*) The length traveled by the hyphal apex over a 20-s interval in the growing hypha shown in *A* is shown in total period of 600 s. (*D*) Sequence of PALM images of mEosFP*thermo*-ChsB reconstructed by moving window binning (500 frames each with a shift increment of 50 frames or 2.5 s, total 140 s). (Scale bar, 1 μm.) (*E*) Overlay of cell profiles from a series of six PALM images expressing hypha. Larger extensions of the apical membrane were indicated by arrows. (Scale bar, 300 nm.) (*F*) Fluorescence image sequence of F-actin and the SV visualized by GFP-TpmA and mCherry-ChsB, respectively, in the growing hypha. The elapsed time is given in seconds. (Scale bar, 2 μm.) (*G*) Kymographs of F-actin (green) and SV (red) along the growth axis in the growing hypha in *F*. Total 180 s. (*H*) Fluorescence intensity of F-actin (green) and SV (red) along the apex of the growing hypha between dotted lines in *G*. (*I*) Normalized cross-correlation of F-actin signal (GFP-TpmA) and SV signal (mCherry-ChsB).

tip, and time-resolved recording and frame analysis by kymographs revealed that the signal intensity oscillated (Fig. 1 *F* and *G* and Movie S2). The line profiles corresponding to the signal intensity of F-actin (green) and SV (red) indicated oscillations with peaks at similar times (Fig. 1*H*). The mean interval of the intensity of F-actin peaks was 29 ± 8 s (n = 50 peaks in 20 hyphae), whereas the mean interval of peaks of the SV was comparable to the one of F-actin, 30 ± 7 s (n = 50 peaks in 20 hyphae). To determine the temporal relationship between the presence of F-actin and the SV, we calculated the normalized cross-correlation of their signal intensities (Fig. 1*I* and Fig. S1*C*). The value at the central peak is 0.50, indicative of a positive correlation between the signals of F-actin (Fig. 1*H*, green) and the SV (Fig. 1*H*, red) (1 and –1 represent perfect positive and negative correlation, respectively). There were a few second delays in the signals of the SV in comparison with the signals of F-actin. These results indicate that SV accumulate during actin polymerization phases and SV are depleted because of exocytosis during actin depolymerization. The distance of tip extension (measured every 20 s) and the SV signal showed a negative correlation (Fig. S1*D*).

Negative Correlation Between the SV Amount at Hyphal Tips and the Cell-Extension Rate. Another model filamentous fungus, *Neurospora crassa*, is advantageous for cell imaging because of its larger cell size, faster cell-extension rate, and more distinct Spitzenkörper (20). The cell-extension rate of *N. crassa* was ∼10 times faster (0.2 μm/s) than the one of *A. nidulans* (Fig. 2 *A* and *B* and Movie S3) and oscillated between 0.15 and 0.45 μm/s (see below). GFP-tagged chitin synthase class III (CHS-1) continuously localized to the Spitzenkörper at the hyphal tip (Fig. 2*A*) (34). The signal intensity of CHS-1–GFP at the Spitzenkörper was displayed in a kymograph along the growth axis (Fig. 2*B*). The line graph indicates oscillations of the GFP intensity (Fig. 2*C*). The mean period between peaks was 17 ± 6 s (n = 30 peaks in 4 hyphae) (Fig. 2*D*).

The signal intensity of CHS-1–GFP at the Spitzenkörper and the hyphal cell-extension rate were measured every 2 s (Fig. 2*E*). When the GFP intensity increased, the cell-extension rate decreased, whereas a decrease in the GFP intensity was accompanied by an increase in the cell-extension rate. Normalized cross-correlation analysis yielded a clear negative correlation between CHS-1–GFP intensity and cell-extension rate, with a value of –0.54 at the central peak (Fig. 2*F*). These results again reveal that SV accumulate at the hyphal tip during slow growth phases and that the SV amount decreases by active exocytosis during fast growth phases. Sometimes, the Spitzenkörper moved from the center of the hyphal apex to the left or to the right; up and down movement was not resolved in our experiment (Fig. S1*E*). Whereas the cell-extension rate in *N. crassa* was ∼10 times faster than that of *A. nidulans*, the oscillation period of SV accumulation of *N. crassa* was half that of *A. nidulans*. It appears that faster growing hyphae exhibit shorter oscillation periods of their cell extension (2).

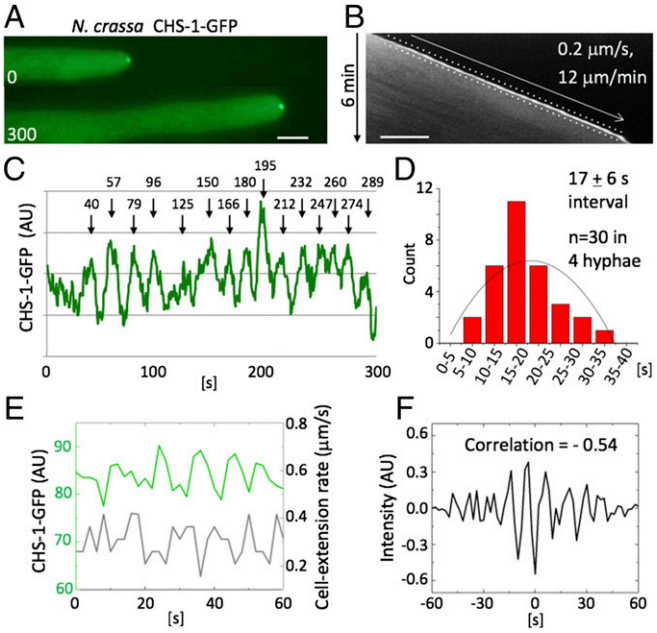

Fig. 2. Negative correlation between SV accumulation and the cell-extension rate in *N. crassa*. (*A*) Fluorescence image sequence of SV visualized by CHS-1-GFP in growing hypha of *N. crassa*. The elapsed time is given in seconds. (Scale bar, 10 μm.) (*B*) Kymograph of SV accumulation along the growth axis in the growing hypha in *A*. Total 300 s. (Scale bar, 10 μm.) (*C*) Fluorescence intensity of SV along the apex of the growing hypha between dotted lines in *B*. Arrows and numbers indicate the time of peaks. (*D*) Distribution of interval between two peaks. n = 30 in 3 hyphae. (*E*) Fluorescence intensity of the SV at the apex (green) and growth rate (gray) every 2 s. The growth rates were calculated by distance of tip position between 2 s. (*F*) Normalized cross-correlation of SV signal (CHS-1–GFP) and cell-extension rate.

Intracellular Ca^{2+} Oscillation Synchronizes Actin Polymerization and SV Accumulation. Intracellular Ca^{2+} levels regulate actin assembly and vesicle fusion (7, 8). The red-fluorescent Ca^{2+} biosensor R-GECO was produced in *A. nidulans*. No obvious morphological changes of the cells because of the expression of the foreign protein were observed under the tested conditions. R-GECO emission varies with the concentration of Ca^{2+} (Fig. S2*A*) (35). When grown in media supplemented with 1 μM $CaCl_2$, pulses of the R-GECO signal were observed (Fig. 3*A* and Movie S4). The R-GECO pulses in Fig. 3*A* were visualized in a kymograph as sharp lines and quantified in a line graph (Fig. 3 *B* and *C*). The mean interval between peaks was 26 ± 7 s (n = 52 peaks in 15 hyphae) (Fig. 3*D*), comparable to the one of F-actin and the SV (Fig. 1*F*). The R-GECO signal appeared as a tip-high gradient and diffused backward (Fig. S2 *B* and *C*). Each hypha showed the signal with different timing (Fig. S2*D*). Such R-GECO pulses continued for multiple times before they disappeared (maximum n = 8 in 180 s), probably because of a limited turnover of R-GECO. The fluorescence of R-GECO could not be detected in media without $CaCl_2$ or with 1 μM $CaCl_2$ + 10 mM EGTA (Fig. S3 *A* and *B*), indicating that the increase of the intracellular Ca^{2+} level is induced by the influx of Ca^{2+} to the cells at hyphal tips. R-GECO pulses were observed with this method in rapidly growing hyphae but not in germlings.

We compared the signals of R-GECO and GFP-TpmA (F-actin) or BglA-GFP (β-glycosidase, secreted protein as a marker for the SV) (22). The fungal cells producing R-GECO and GFP-TpmA, cultured in medium supplemented with 1 μM $CaCl_2$, showed oscillating signals of GFP and R-GECO (Fig. 3*E* and Movie S5). Kymographs along the growth axis indicated temporal changes of signal intensities (Fig. 3*E*). Line profiles corresponding to the signal intensities of F-actin (Fig. 3*E*, green) and the Ca^{2+} concentration (Fig. 3*E*, red) at the tip indicated that oscillations of peak intensities had similar periods (29 ± 8 and 26 ± 7 s, respectively) and were synchronized (Fig. 3*F*). Normalized cross-correlation analysis yielded a positive correlation between the concentrations of F-actin (Fig. 3*F*, green) and Ca^{2+} (Fig. 3*F*, red), with the central peak at 0.40 (Fig. 3*G*) and indicated that the peaks of Ca^{2+} appeared a few seconds earlier than those of F-actin. These results are in agreement with the notion that Ca^{2+} influx at the growing hypha induces actin depolymerization.

Hyphae producing R-GECO and BglA-GFP (SV) showed oscillations of the GFP intensity at the tip and R-GECO pulses (Fig. 3*H* and Movie S6), with similar periods (30 ± 7 and 26 ± 7 s, respectively), which were synchronized (Fig. 3*I*). Normalized cross-correlation analysis yielded a positive correlation with a

MICROBIOLOGY

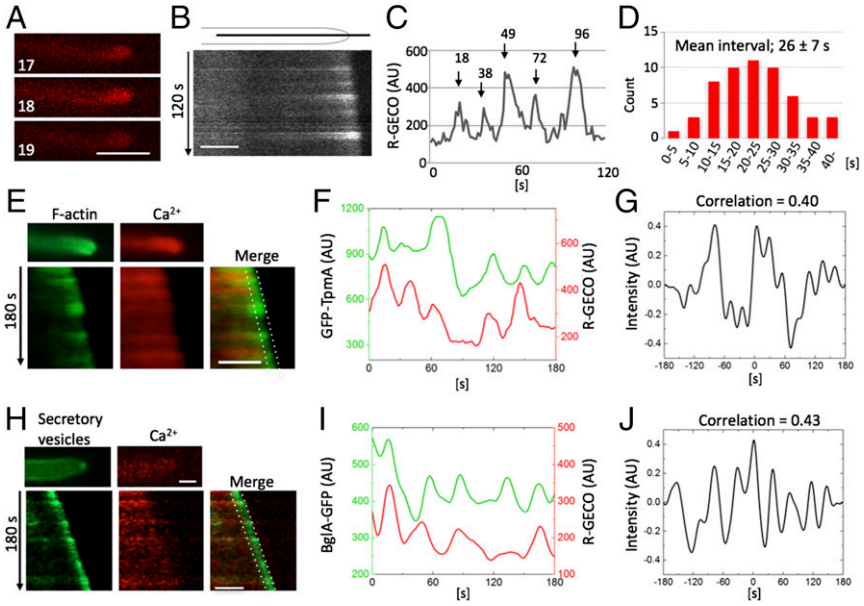

Fig. 3. Oscillation of Ca^{2+} influx correlated with F-actin and the SV. (*A*) Fluorescence image sequence of R-GECO. The elapsed time is given in seconds. (Scale bar, 5 μm.) (*B*) Kymograph along the hypha shown in *A*. Total 120 s. (Scale bar, 5 μm.) (*C*) Fluorescence intensity around the tip of hypha in *B* is plotted. Arrows and numbers indicate the time of Ca^{2+} peaks. (*D*) Distribution of intervals between two peaks. $n = 36$ in 10 hyphae. (*E*) Fluorescence images and kymographs along the growth axis of F-actin (GFP-TpmA; green) and Ca^{2+} (R-GECO; red). Total 180 s. (Scale bar, 2 μm.) (*F*) Fluorescence intensity of F-actin (green) and Ca^{2+} (red) along the apex of the growing hypha between dotted lines in *E*. (*G*) Normalized cross-correlation of F-actin signal (GFP-TpmA) and Ca^{2+} signal (R-GECO). (*H*) Fluorescence images and kymographs along the growth axis of SV (BglA-GFP; green) and Ca^{2+} (R-GECO; red). Total 180 s. (Scale bars, 1 μm.) (*I*) Fluorescence intensity of SV (green) and Ca^{2+} (red) along the apex of the growing hypha between dotted lines in *H*. (*J*) Normalized cross-correlation of SV signal (BglA-GFP) and Ca^{2+} signal (R-GECO).

central peak value of 0.43 (Fig. 3*J*) and a few seconds delay of BglA-GFP. These results indicate that Ca^{2+} influx affords exocytosis mediated by fusion of the SV with the plasma membrane, as well as actin depolymerization.

Ca^{2+} Channels Coordinate Ca^{2+} Influx, Actin Polymerization, and Cell-Extension Rate. Several Ca^{2+} channels, pumps, and transporters function in different organelles, such as the plasma membrane, endoplasmic reticulum, Golgi, mitochondria, and vacuole in fungi (36). The Ca^{2+} channels at the plasma membrane, Mid1 and Cch1p, of *Saccharomyces cerevisiae* share the single pathway that responds to environmental stresses and ensures cellular Ca^{2+} homeostasis (37–39). Deletion of these orthologs in *A. nidulans*, *midA* and *cchA*, caused a defect in polarized growth and cell wall synthesis (40). Deletion of *midA* or *cchA* often caused abnormal branching and de-polarized hyphae (Fig. 4*A* and Fig. S3*C*), and addition of 10 mM $CaCl_2$ partially restored normal morphology.

Fluorescence imaging showed no pulse of R-GECO fluorescence in the *midA*- or *cchA*-deletion strain grown in the media supplemented with 1 μM $CaCl_2$, and no oscillation of actin polymerization determined by GFP-TpmA fluorescence (Fig. 4*B* and Fig. S3*D*), in contrast to the wild-type (Fig. 3*E*). No oscillation of the cell-extension rate was apparent (Fig. 4*C*), and cell extension in the deletion strain was too slow for microscopy to show the oscillations of the hyphal tip extension. Addition of 10 mM $CaCl_2$ occasionally caused Ca^{2+} entry into the deletion strains, but restored neither the oscillation of Ca^{2+} influx nor the oscillation of actin polymerization (Fig. 4*D*). Ca^{2+} influx and actin polymerization in the wild-type strain remained oscillatory in the presence of 10 mM $CaCl_2$ (Fig. S3*E*). These results indicate that pulsed Ca^{2+} influx effected by Ca^{2+} channels is required for the oscillation of actin polymerization and the cell-extension rate, resulting in proper polarized growth of hyphae, which is also supported by the result that the treatment of calcium ionophore A23187 disrupted the oscillation of Ca^{2+} and actin polymerization and caused swollen hyphal tips by depolarized growth (Fig. S3*F*).

Discussion

The hyphal tip of filamentous fungi comprises an excellent model to investigate polarity determination and maintenance, as well as polar cell growth, which occurs in a pulsed fashion. We were able to simultaneously analyze actin polymerization, SV fusion, and the intracellular Ca^{2+} concentration. Our findings

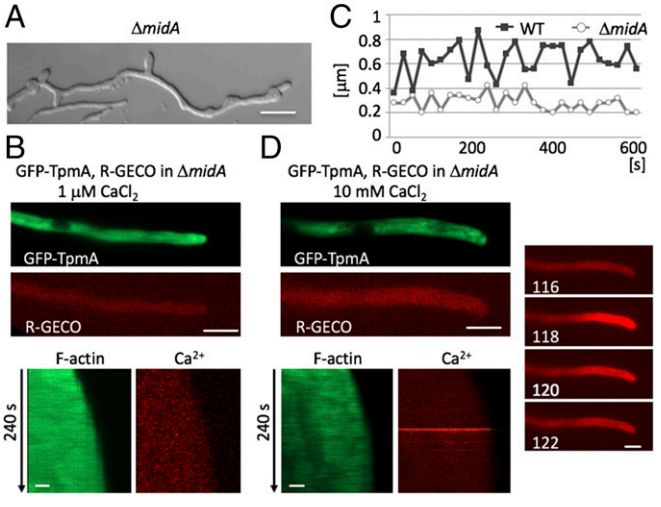

Fig. 4. Deletion of Ca^{2+} channel. (*A*) Hyphal morphology of the *midA* deletion strain. (Scale bar, 20 μm.) (*B*) Fluorescence images of GFP-TpmA and R-GECO in the *midA*-deletion hyphae growing in the media with 1 μM $CaCl_2$. (Scale bar, 10 μm.) (*C*) The length traveled by the hyphal apex over a 20-s interval in the wild-type and *midA*-deletion strain. Total period of 600 s. (*D*) Fluorescence images of GFP-TpmA and R-GECO in the *midA*-deletion hyphae growing in the media with 10 mM $CaCl_2$ (*Upper*) and time course of R-GECO (*Left*). (Scale bars, *Upper* and *Right*, 5 μm.) Kymographs along the hyphae in *B* and *D*. Total 240 s, every 2 s. (Scale bar, *Bottom*, 1 μm.)

can be summarized in the following model (shown in Fig. 5). During slow growth phases (i.e., low exocytosis activity), polymerized actin filaments accumulate at the hyphal tips, followed by SV accumulation before exocytosis. The transient increase of the intracellular Ca^{2+} level as a result of Ca^{2+} influx causes depolymerization of actin and fusion of the SV with the plasma membrane, resulting in more exocytosis and fast cell-extension phases. Reports that Ca^{2+} levels induce actin depolymerization and vesicle fusion in vitro support our model (7, 8). Similar oscillation periods of Ca^{2+} influx, actin polymerization, and SV accumulation at the tips of *A. nidulans* (~30 ± 8 s) (Figs. 1*H* and 3 *F* and *I*) indicate that the cells coordinate these processes during stepwise cell extension. A few seconds of delay between these processes indicate that Ca^{2+} influx, actin depolymerization, and SV fusion are sequential mechanisms that proceed in this order to extend the cell periphery at the hyphal tips. Negative correlation between the oscillation peaks of the SV amounts and the cell-extension rate without a time gap (Fig. 2*E*) is consistent with the notion that exocytosis activity limits cell extension. This model is in agreement with our recent transient polarity assembly model of fungal tip growth, which describes the assembly/disassembly of polarity markers, polymerization of actin, and local exocytosis resulting in local membrane extension (18, 22, 23).

Here we demonstrate that normal oscillation of actin polymerization and stepwise growth require pulses of Ca^{2+} influx through the Ca^{2+} channels, CchA and MidA, in *A. nidulans*. The key event hence appears to be the activation of Ca^{2+} channels. One attractive possibility is that the Ca^{2+} channels could be stretch-activated. During slow growth phases cells gradually build up turgor pressure against the membrane and the cell wall. When the membrane tension exceeds a threshold, the Ca^{2+} channels could be activated. Following the entry of Ca^{2+}, exocytosis is promoted and leads to cell extension, which in turn decreases the turgor pressure and inactivates the channels. Indeed, stretch activation of the *S. cerevisiae* ortholog Mid1 has been reported (41). Another simple possibility is that the calcium channel firing is refractory to further activation until the cytoplasmic Ca^{2+} level is restored to resting levels by diffusion or efflux. The oscillation of the cytoplasmic Ca^{2+} level might also play a role in other physiological processes as well and not only for hyphal tip growth.

Our oscillatory model of cell growth implies a transient waiting time of SV before exocytosis. This raises the question about an advantage of pulsed versus continuous growth. Massive exocytosis at hyphal tips, which is the basis for rapid hyphal growth, imposes a huge problem for polarity maintenance. The newly inserted membrane dilutes locally polarity markers and the exocytosis machinery (i.e., the exocyst complex and SNARE proteins), which serve to direct vesicles to specific locations on the plasma membrane and to mediate their tethering to the membrane immediately before fusion (22, 42). If the number of fused vesicles exceeds the capacity of the cell to assemble focused polarity sites, the polar marker would diffuse on the plasma membrane. This has been nicely shown in *S. cerevisiae* (42). The waiting time of the SV till the next exocytosis event may allow the polarity components to rearrange at newly forming polarity sites and thus assemble enough actin cables that serve as tracks for directed vesicle transport (16, 19). In contrast, cortical actin meshes anchor the vesicles and, at the same time, function as barriers for vesicle fusion with the plasma membrane in mammalian cells (4). The transient increase of the intracellular Ca^{2+} level by Ca^{2+} influx is likely to be an important signal to coordinate depolymerization of actin meshes and thereby allow the anchored SV to fuse with the plasma membrane for exocytosis.

Our data reveal correlations among oscillations of four cell peripheral machineries of cell extension, F-actin, exocytosis, and Ca^{2+} levels, and provide comprehensive understanding of pulsed cell extension at the molecular level. Coordinated cycles or oscillations of these machineries are expected to be ubiquitous in all eukaryotes. Indeed, oscillations of intracellular Ca^{2+} levels and actin polymerization have been revealed in mammalian and plant cells (4–6). Although the time needed for assembly of polarity markers may be one reason for oscillatory growth, it may also be a mechanism for the cells to respond more quickly to both internal and environmental cues, including chemical and mechanical stimuli. Indeed, Ca^{2+} influx by the Ca^{2+} channel Cch1 in *Candida albicans* is involved in the control of directional growth of hyphae (43). The stepwise growth coordinated by transient Ca^{2+} influx could link growth with chemotropism and chemotaxis. Oscillatory recruitment of MAP kinase to cell tips during cell fusion in *N. crassa* is also involved in the process (44).

Because filamentous fungi maintain the growth site at their hyphal tips, this system is ideal for elucidating the mechanism of pulsed growth. Further analysis of the contribution of other processes, such as endocytosis, cell signaling, cell wall synthesis, and turgor pressure, will be necessary to complete the picture.

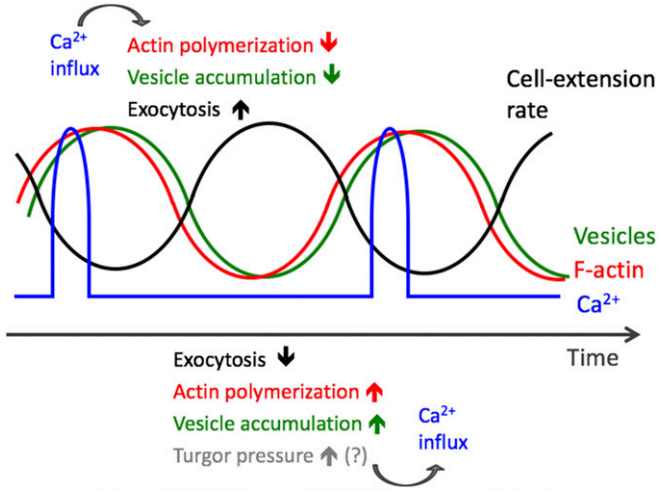

Fig. 5. Scheme of oscillation in fungal tip growth coordinated by Ca^{2+} influx.

Materials and Methods

Strains, Plasmids, and Culture Conditions. Supplemented minimal medium for *A. nidulans* was prepared as described, and standard strain construction procedures were used (45). Two percent of glucose was used as carbon source; 70 mM sodium nitrate and 0.9 μM ammonium molybdate were used as nitrogen source for solid media, if not stated otherwise. For liquid media, the carbon sources were 2% glucose, 2% threonine, or 2% glycerol. *A. nidulans* strains used in this study are listed in Table S1. Standard laboratory *Escherichia coli* strains (Top 10 F′) were used. *N. crassa* (CHS-1–GFP) strain was grown on Vogel's minimal medium agar at 32 °C for 3 d and observed using the "inverted agar block method" (46).

Plasmid and Strain Construction. The sequence of R-GECO was amplified from plasmid pPD60 RGECO.1 (35), using primers R-GECO-KpnI-fw and R-GECO-XbaI-r, generating KpnI and XbaI restriction enzyme sites, respectively, and subsequently cloned into plasmid pJET1.2. The constructed plasmid was further digested with KpnI and XbaI and the corresponding to R-GECO ORF band was gel-extracted, purified, and cloned in the KpnI-XbaI–digested pCMB17apx (for proteins of interest expressed under the regulatable *alcA* promoter; contains *N. crassa* pyr-4) (21) plasmid downstream of the *alcA* promoter sequence, yielding pNT76. The DNA fragment for GFP tagging at the C terminus of BglA was amplified by fusion-PCR with a GFP-pyrG cassette (47) using primers BglA_P1, BglA_P2, BglA_P3, BglA_P5, and BglA_P6, and was subsequently cloned into plasmid pJET1.2, yielding pNG3. The sequence of *chsB* was amplified from genomic DNA by using primers chsB_AscI_fwd and chsB_PacI_rev, was digested with AscI and PacI, and cloned into the AscI-PacI–digested pSH44 (for mCherry tagging at N terminus of proteins of

MICROBIOLOGY

interest expressed under the regulatable *alcA* promoter; contains *pyroA*) (48), yielding pNT77. The AscI-PacI–digested *chsB* sequence was replaced with the *teaR* sequence in pNT65 (for mEosFP*thermo* tagging at N terminus of proteins of interest expressed under the regulatable *alcA* promoter; contains *pyr-4*) (22), yielding pNT75. The plasmids were transformed into the TN02A3 strain (49). Transformants were screened microscopically for fluorescence and confirmed by PCR for correct integration of the constructs. The plasmids and primers used in this study are listed in Tables S2 and S3.

Fluorescence Microscopy. Cells were grown in eight-well glass-bottom slides (Ibidi) with minimal medium at 28 °C overnight. Images were captured using an Axiophot microscope using a Plan-Apochromatic 63× 1.4 Oil objective lens, the ZEISS AxioCam MRM camera (Zeiss), and the HBO 103 mercury arc lamp (Osram) or HXP 120 (Zeiss), featuring faster wavelength switching. Images were collected and analyzed by using the Zen system (Zeiss) and ImageJ software. Photobleaching corrections were not applied to the data.

Super-Resolution Microscopy. PALM images were acquired at room temperature on a modified inverted microscope (Axiovert 200, Zeiss) as described previously (22). The fluorescent proteins were converted from their green to red emitting forms using a 405-nm laser (Stradus 405-250, Vortran Laser Technology) with an intensity of 0–50 W/cm^2. Fluorescence was excited by a 561-nm laser (Gem 561, Laser Quantum) with simultaneous 405-nm illumination (200–400 W/cm^2). PALM images were analyzed with custom-written analysis software, a-livePALM (50) running under the MATLAB R2015b (The Mathworks) environment.

ACKNOWLEDGMENTS. We thank our laboratory members for valuable discussion and critical reading of the manuscript, and B. Schreckenberger and E. Wohlmann for excellent technical assistance. This work was supported by the Deutsche Forschungsgemeinschaft Grants (TA819/2-1, FOR1334, NI291/12-1, and GRK2039), the Helmholtz Association Program STN, the Japan Society for the Promotion of Science KAKENHI Grant 15K18663, and the Japan Science and Technology Agency Exploratory Research for Advanced Technology (ERATO) Grant JPMJER1502.

1. Das M, et al. (2012) Oscillatory dynamics of Cdc42 GTPase in the control of polarized growth. *Science* 337:239–243.
2. López-Franco R, Bartnicki-Garcia S, Bracker CE (1994) Pulsed growth of fungal hyphal tips. *Proc Natl Acad Sci USA* 91:12228–12232.
3. Winans AM, Collins SR, Meyer T (2016) Waves of actin and microtubule polymerization drive microtubule-based transport and neurite growth before single axon formation. *eLife* 5:e12387.
4. Wollman R, Meyer T (2012) Coordinated oscillations in cortical actin and Ca2+ correlate with cycles of vesicle secretion. *Nat Cell Biol* 14:1261–1269.
5. Monshausen GB, Messerli MA, Gilroy S (2008) Imaging of the Yellow Cameleon 3.6 indicator reveals that elevations in cytosolic Ca2+ follow oscillating increases in growth in root hairs of *Arabidopsis*. *Plant Physiol* 147:1690–1698.
6. Holdaway-Clarke TL, Feijo JA, Hackett GR, Kunkel JG, Hepler PK (1997) Pollen tube growth and the intracellular cytosolic calcium gradient oscillate in phase while extracellular calcium influx is delayed. *Plant Cell* 9:1999–2010.
7. Janmey PA (1994) Phosphoinositides and calcium as regulators of cellular actin assembly and disassembly. *Annu Rev Physiol* 56:169–191.
8. Schneggenburger R, Neher E (2005) Presynaptic calcium and control of vesicle fusion. *Curr Opin Neurobiol* 15:266–274.
9. Fischer R, Zekert N, Takeshita N (2008) Polarized growth in fungi—Interplay between the cytoskeleton, positional markers and membrane domains. *Mol Microbiol* 68: 813–826.
10. Takeshita N, Manck R, Grün N, de Vega SH, Fischer R (2014) Interdependence of the actin and the microtubule cytoskeleton during fungal growth. *Curr Opin Microbiol* 20:34–41.
11. Riquelme M, et al. (2011) Architecture and development of the *Neurospora crassa* hypha—A model cell for polarized growth. *Fungal Biol* 115:446–474.
12. Egan MJ, McClintock MA, Reck-Peterson SL (2012) Microtubule-based transport in filamentous fungi. *Curr Opin Microbiol* 15:637–645.
13. Pantazopoulou A, Pinar M, Xiang X, Peñalva MA (2014) Maturation of late Golgi cisternae into RabE(RAB11) exocytic post-Golgi carriers visualized in vivo. *Mol Biol Cell* 25:2428–2443.
14. Taheri-Talesh N, Xiong Y, Oakley BR (2012) The functions of myosin II and myosin V homologs in tip growth and septation in *Aspergillus nidulans*. *PLoS One* 7:e31218.
15. Zhang J, et al. (2011) *Aspergillus* myosin-V supports polarized growth in the absence of microtubule-based transport. *PLoS One* 6:e28575.
16. Taheri-Talesh N, et al. (2008) The tip growth apparatus of *Aspergillus nidulans*. *Mol Biol Cell* 19:1439–1449.
17. Horio T, Oakley BR (2005) The role of microtubules in rapid hyphal tip growth of *Aspergillus nidulans*. *Mol Biol Cell* 16:918–926.
18. Bergs A, Ishitsuka Y, Evangelinos M, Nienhaus GU, Takeshita N (2016) Dynamics of actin cables in polarized growth of the filamentous fungus *Aspergillus nidulans*. *Front Microbiol* 7:682.
19. Berepiki A, Lichius A, Read ND (2011) Actin organization and dynamics in filamentous fungi. *Nat Rev Microbiol* 9:876–887.
20. Riquelme M, Sánchez-León E (2014) The Spitzenkörper: A choreographer of fungal growth and morphogenesis. *Curr Opin Microbiol* 20:27–33.
21. Takeshita N, Higashitsuji Y, Konzack S, Fischer R (2008) Apical sterol-rich membranes are essential for localizing cell end markers that determine growth directionality in the filamentous fungus *Aspergillus nidulans*. *Mol Biol Cell* 19:339–351.
22. Ishitsuka Y, et al. (2015) Superresolution microscopy reveals a dynamic picture of cell polarity maintenance during directional growth. *Sci Adv* 1:e1500947.
23. Takeshita N (2016) Coordinated process of polarized growth in filamentous fungi. *Biosci Biotechnol Biochem* 80:1693–1699.
24. Kim HS, et al. (2012) Expression of the Cameleon calcium biosensor in fungi reveals distinct Ca(2+) signatures associated with polarized growth, development, and pathogenesis. *Fungal Genet Biol* 49:589–601.
25. Garcia-Vidal C, Viasus D, Carratalà J (2013) Pathogenesis of invasive fungal infections. *Curr Opin Infect Dis* 26:270–276.
26. Punt PJ, et al. (2002) Filamentous fungi as cell factories for heterologous protein production. *Trends Biotechnol* 20:200–206.
27. Kobayashi T, et al. (2007) Genomics of *Aspergillus oryzae*. *Biosci Biotechnol Biochem* 71:646–670.
28. Betzig E, et al. (2006) Imaging intracellular fluorescent proteins at nanometer resolution. *Science* 313:1642–1645.
29. Hess ST, Girirajan TP, Mason MD (2006) Ultra-high resolution imaging by fluorescence photoactivation localization microscopy. *Biophys J* 91:4258–4272.
30. Takeshita N, et al. (2015) Transportation of *Aspergillus nidulans* class III and V chitin synthases to the hyphal tips depends on conventional kinesin. *PLoS One* 10:e0125937.
31. Wiedenmann J, et al. (2011) From EosFP to mIrisFP: Structure-based development of advanced photoactivatable marker proteins of the GFP-family. *J Biophotonics* 4: 377–390.
32. Wiedenmann J, Nienhaus GU (2006) Live-cell imaging with EosFP and other photoactivatable marker proteins of the GFP family. *Expert Rev Proteomics* 3:361–374.
33. Nienhaus GU, et al. (2006) Photoconvertible fluorescent protein EosFP: Biophysical properties and cell biology applications. *Photochem Photobiol* 82:351–358.
34. Sánchez-León E, et al. (2011) Traffic of chitin synthase 1 (CHS-1) to the Spitzenkörper and developing septa in hyphae of *Neurospora crassa*: Actin dependence and evidence of distinct microvesicle populations. *Eukaryot Cell* 10:683–695.
35. Zhao Y, et al. (2011) An expanded palette of genetically encoded Ca^{2+} indicators. *Science* 333:1888–1891.
36. Zelter A, Bencina M, Bowman BJ, Yarden O, Read ND (2004) A comparative genomic analysis of the calcium signaling machinery in *Neurospora crassa*, *Magnaporthe grisea*, and *Saccharomyces cerevisiae*. *Fungal Genet Biol* 41:827–841.
37. Paidhungat M, Garrett S (1997) A homolog of mammalian, voltage-gated calcium channels mediates yeast pheromone-stimulated Ca2+ uptake and exacerbates the cdc1(Ts) growth defect. *Mol Cell Biol* 17:6339–6347.
38. Iida H, Nakamura H, Ono T, Okumura MS, Anraku Y (1994) MID1, a novel *Saccharomyces cerevisiae* gene encoding a plasma membrane protein, is required for Ca2+ influx and mating. *Mol Cell Biol* 14:8259–8271.
39. Locke EG, Bonilla M, Liang L, Takita Y, Cunningham KW (2000) A homolog of voltage-gated Ca(2+) channels stimulated by depletion of secretory Ca(2+) in yeast. *Mol Cell Biol* 20:6686–6694.
40. Wang S, et al. (2012) Putative calcium channels CchA and MidA play the important roles in conidiation, hyphal polarity and cell wall components in *Aspergillus nidulans*. *PLoS One* 7:e46564.
41. Kanzaki M, et al. (1999) Molecular identification of a eukaryotic, stretch-activated nonselective cation channel. *Science* 285:882–886.
42. Savage NS, Layton AT, Lew DJ (2012) Mechanistic mathematical model of polarity in yeast. *Mol Biol Cell* 23:1998–2013.
43. Brand AC, et al. (2014) Cdc42 GTPase dynamics control directional growth responses. *Proc Natl Acad Sci USA* 111:811–816.
44. Fleissner A, Leeder AC, Roca MG, Read ND, Glass NL (2009) Oscillatory recruitment of signaling proteins to cell tips promotes coordinated behavior during cell fusion. *Proc Natl Acad Sci USA* 106:19387–19392.
45. Hill TW, Kafer E (2001) Improved protocols for *Aspergillus* minimal medium: Trace element and minimal medium salt stock solutions. *Fungal Genet Newsl* 48:20–21.
46. Hickey PC, Swift SM, Roca MG, Read ND (2005) Live-cell imaging of filamentous fungi using vital fluorescent dyes. *Methods Microbiol* 34:63–87.
47. Szewczyk E, et al. (2006) Fusion PCR and gene targeting in *Aspergillus nidulans*. *Nat Protoc* 1:3111–3120.
48. Takeshita N, et al. (2013) The cell-end marker TeaA and the microtubule polymerase AlpA contribute to microtubule guidance at the hyphal tip cortex of *Aspergillus nidulans* to provide polarity maintenance. *J Cell Sci* 126:5400–5411.
49. Nayak T, et al. (2006) A versatile and efficient gene-targeting system for *Aspergillus nidulans*. *Genetics* 172:1557–1566.
50. Li Y, Ishitsuka Y, Hedde PN, Nienhaus GU (2013) Fast and efficient molecule detection in localization-based super-resolution microscopy by parallel adaptive histogram equalization. *ACS Nano* 7:5207–5214.

Supporting Information

Takeshita et al. 10.1073/pnas.1700204114

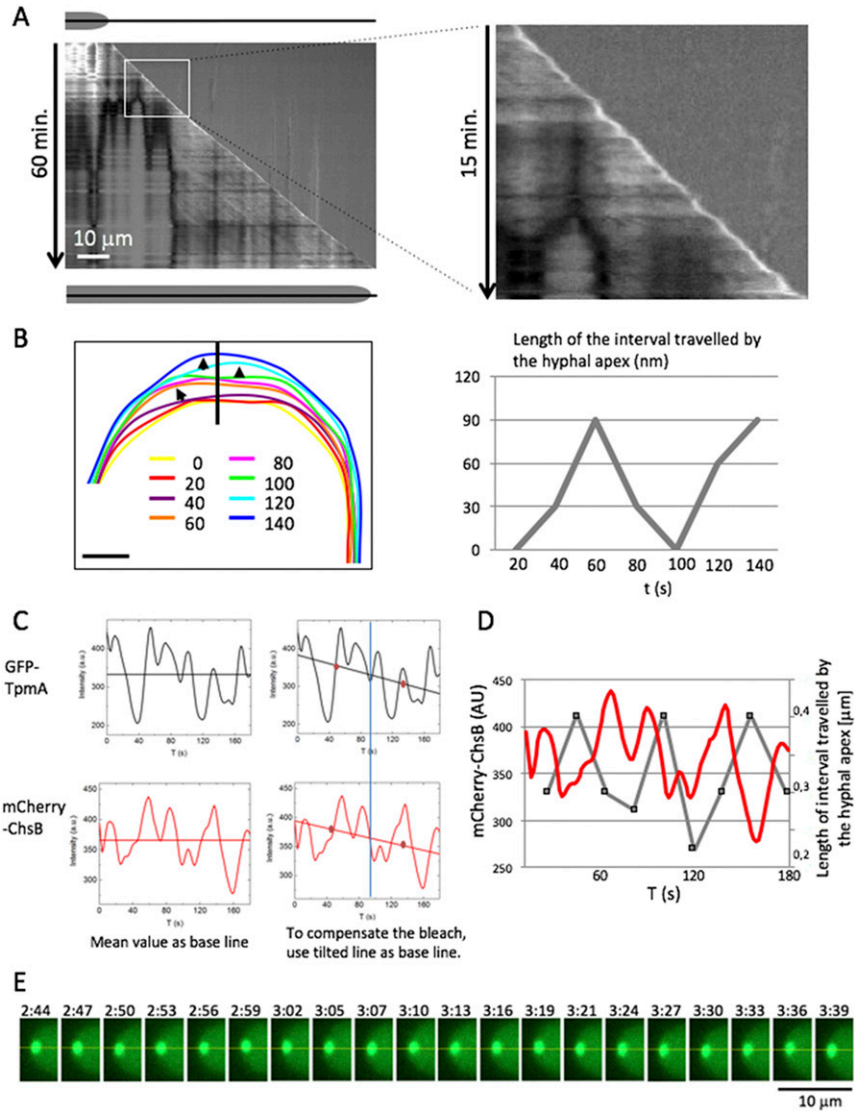

Fig. S1. Stepwise growth of hyphae. (*A*) Kymograph of the growing hypha along the growth axis (*Left*) and enhanced image (Right). Total 60 min. (Scale bar, *Left*, 10 μm.) (*B*) The length of the interval traveled by the hyphal apex along the line in overlay of cell profiles from a series of six PALM images expressing hypha (Fig. 1*E*). Larger extensions of the apical membrane were indicated by arrows. (Scale bar, 300 nm.) (*C*) Cross-correlation between GFP-TpmA and mCherry-ChsB. To account for the effect of photobleaching during imaging (3 min), the baseline of each signal was defined as a line with negative slope, based on the average value of first and second half of the signal. The cross-correlation was then calculated based on the corrected signal. (*D*) Fluorescence intensity of secretory vesicles (red) along the apex of the growing hypha between dotted lines in (Fig. 1*G*). The length of the interval traveled by the hyphal apex was measured every 20 s. (*E*) The position of Spitzenkörper was aligned every 3 s from Movie S3.

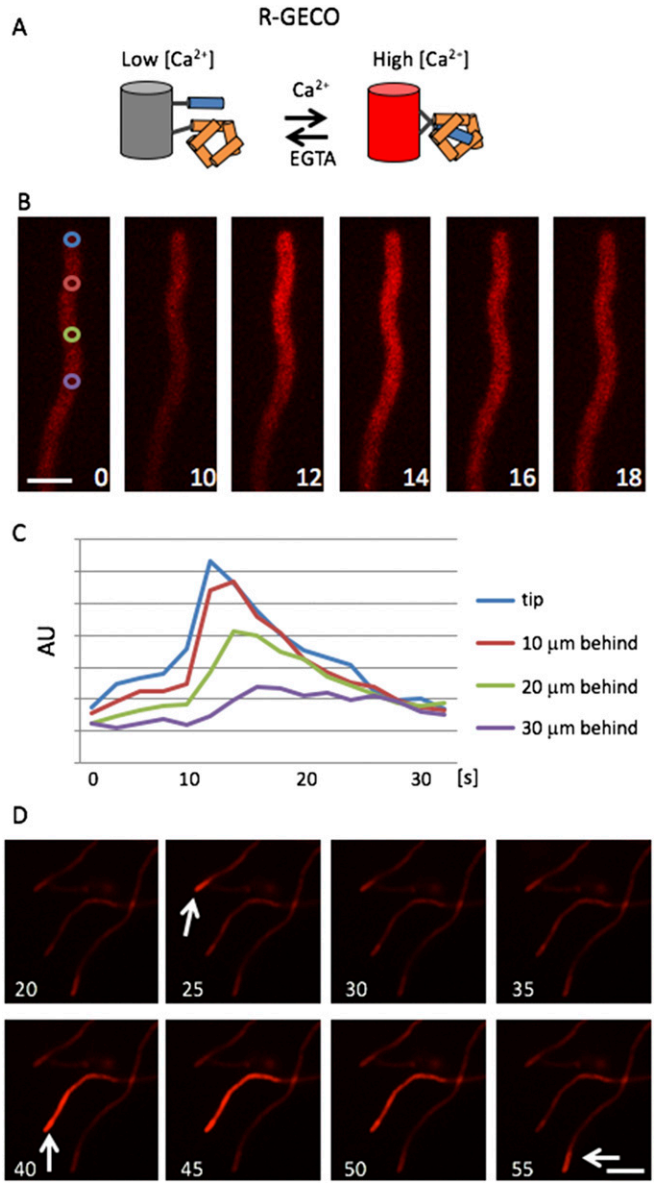

Fig. S2. Intracellular Ca^{2+} level by R-GECO. (*A*) Scheme of the Ca^{2+} biosensor, R-GECO. (*B*) Fluorescence image sequence of R-GECO. The elapsed time is given in seconds. (Scale bar, 5 μm.) (*C*) The time-lapse signal intensity of R-GECO at different points from the tip shown in *B*. (*D*) Fluorescence image sequence of R-GECO in the three hyphae. Arrows indicate hypha showing the R-GECO signal with different timing. The elapsed time is given in seconds. (Scale bar, 10 μm.)

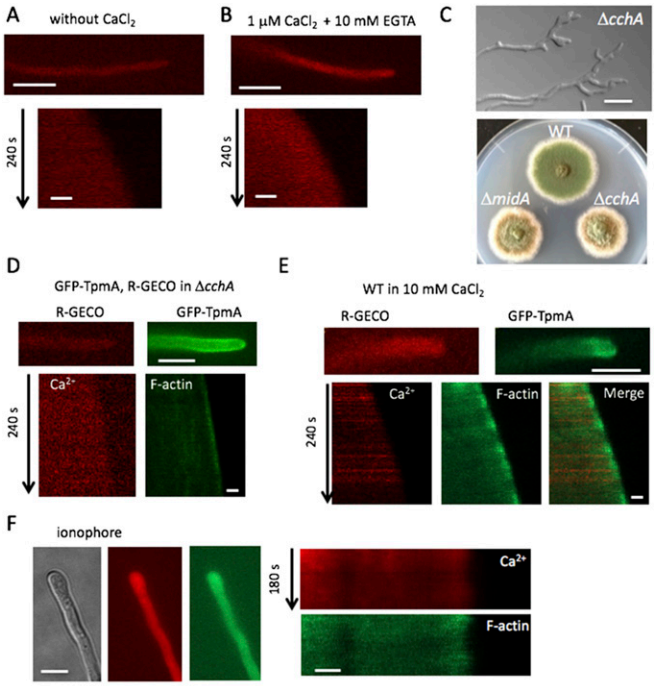

Fig. S3. Effect of $CaCl_2$ on the oscillation of R-GECO. (*A* and *B*) Fluorescence image of R-GECO in the hypha growing in the media without $CaCl_2$ (*A*) and 1 μM $CaCl_2$ + 10 mM EGTA (*B*). (Scale bars, 10 μm.) Kymographs (*Lower*) along the hyphae. Total 240 s, every 2 s. (Scale bars, 1 μm.) (*C*, *Upper*) Hyphal morphology of the *cchA*-deletion strain. (Scale bar, 20 μm.) (*Lower*) Colonies of wild-type, *midA*-deletion and *cchA*-deletion strain grown on the minimal media plate for 3 d. (*D* and *E*) Fluorescence image of R-GECO and GFP-TpmA, in the *cchA*-deletion hyphae growing in the media with 1 μM $CaCl_2$ (*D*), and in the wild-type hypha growing in the media with 10 mM $CaCl_2$ (*E*). (Scale bars, 5 μm.) (*Lower*) Kymographs along the hypha. Total 240 s, every 2 s. (Scale bars, 1 μm.) (*F*) Fluorescence image of R-GECO and GFP-TpmA in the wild-type hypha growing in the media with 1 μM $CaCl_2$ after the treatment of calcium ionophore A23187 (Sigma) 5 μg/mL for 30 min. (Scale bars, 5 μm.)

Table S1. *Aspergillus nidulans* strains used in this study

Strain	Genotype	Source
TN02A3	*pyrG89; argB2; ΔnkuA::argB; pyroA4*	Nayak et al. (49)
SNT147	*pyrG89; argB2; ΔnkuA::argB; pyroA4; [alcA(p)-gfp-tpmA::pyr-4]*	Bergs et al. (18)
CIA08	*pyrG89; riboB2; argB2; ΔnkuA::argB; pyroA4; [ΔmidA::pyrG]*	Wang et al. (40)
WSA05	*pyrG89; riboB2; argB2; ΔnkuA::argB; pyroA4; [ΔcchA::pyrG]*	Wang et al. (40)
SNG10	*pyrG89; argB2; ΔnkuA::argB; pyroA4; [bglA-gfp::pyr-4]*	Present study
SNT167	*pyrG89; argB2; ΔnkuA::argB; pyroA4; [alcA(p)-mEeosthermofp-chsB::pyr-4]*	Present study
SNT161	*pyrG89; argB2; ΔnkuA::argB; pyroA4; [alcA(p)-gfp-tpmA::pyr-4] ; [alcA(p)-mcherry-chsB::pyroA]*	Present study
SNT162	*pyrG89; argB2; ΔnkuA::argB; pyroA4 ; [alcA(p)-R-GECO::pyr-4]*	Present study
SNT163	*pyrG89; argB2; ΔnkuA::argB; pyroA4; [pyroA] [alcA(p)-gfp-tpmA::pyr-4] ; [alcA(p)-R-GECO::pyr-4]*	Present study
SNT164	*pyrG89; argB2; ΔnkuA::argB; pyroA4; [pyroA] [bglA-gfp::pyr-4] ; [alcA(p)-R-GECO::pyr-4]*	Present study
SNT165	*pyrG89; riboB2; argB2; ΔnkuA::argB; pyroA4; [ΔmidA::pyrG]; [pyroA]; [alcA(p)-gfp-tpmA::pyr-4]; [alcA(p)-R-GECO::pyr-4]*	Present study
SNT166	*pyrG89; riboB2; argB2; ΔnkuA::argB; pyroA4; [ΔcchA::pyrG]; [pyroA]; [alcA(p)-gfp-tpmA::pyr-4]; [alcA(p)-R-GECO::pyr-4]*	Present study

Table S2. Plasmids used in this study

Plasmid	Description	Source
pPD60	RGECO.1	Zhao et al. (35)
pNT77	*alcA(p)-mcherry-chsB::pyroA*	Present study
pNG3	*bglA-gfp::pyr-4*	Present study
pNT76	*alcA(p)-R-GECO::pyr-4*	Present study

Table S3. Primers used in this study

Primer	Sequence (5′ → 3′)
RGECO-KpnI-fw	gcggtaccATGGTCGACTCATCACGTCG
RGECO-XbaI-r	gctctagaCTACTTCGCTGTCATCATTTG
BglA_P1	GCGGTGACGGACAACTG
BglA_P2	CAAGACCGCGTCTGAGTCTAC
BglA_P3	tggccgcgttggccAGAGGAAGCTTGCGTGAGG
BglA_P5	GACGGACATGCATGCTAGCAC
BglA_P6	GCATACAGAGGAAACACGCT
chsB_AscI_fwd	cggcgcgcctATGGCCTACCACGGCTC
chsB_PacI_rev	cttaattaattaGGCAACACACTGACATATCC

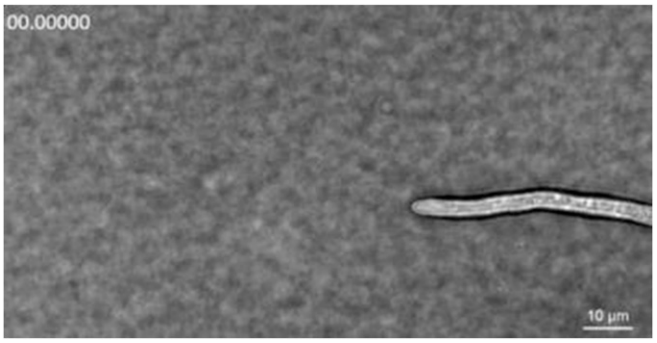

Movie S1. Image sequences of the DIC *A. nidulans* wild-type hyphae growing in the minimal media at 28 °C; every 10 s, total 1,800 s. (Scale bar, 10 μm.) See Fig. 1*A*.

Movie S1

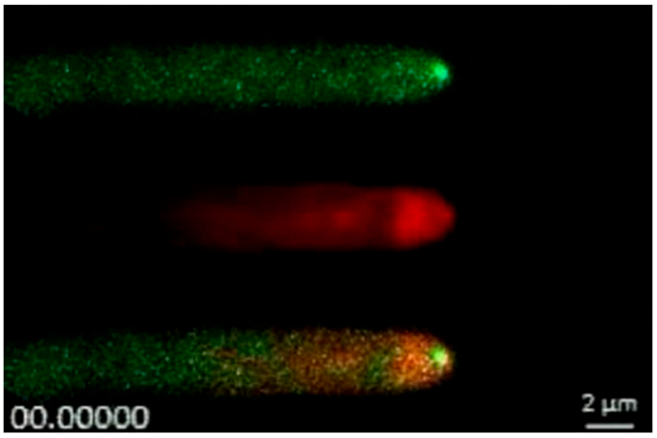

Movie S2. Image sequences of GFP-TpmA and mCherry-ChsB; every 2 s, total 180 s. (Scale bar, 2 μm.) See Fig. 1*F*.

Movie S2

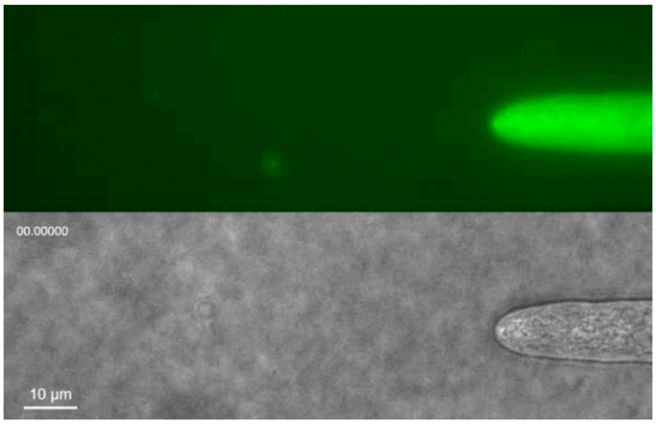

Movie S3. Image sequences of DIC and CHS-1- GFP in *Neurospora crassa*; every 2 s, total 600 s. (Scale bar, 10 μm.) See Fig. 2*A*.

Movie S3

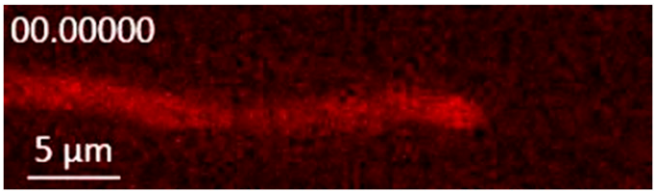

Movie S4. Image sequences of R-GECO; every 1 s, total 120 s. (Scale bar, 5 μm.) See Fig. 2*B*.

Movie S4

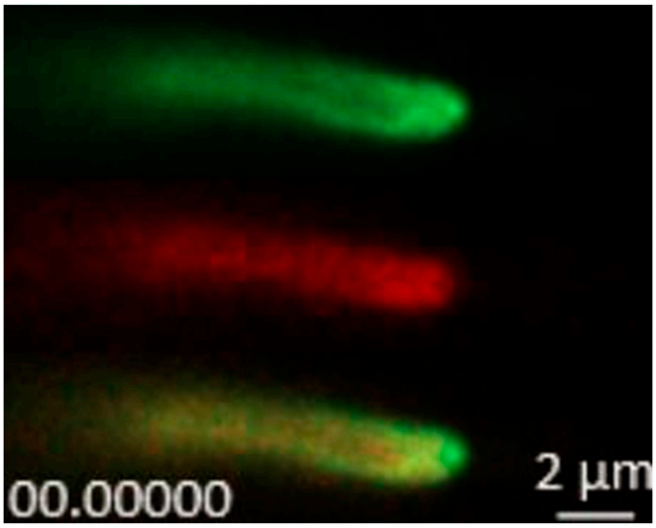

Movie S5. Image sequences of GFP-TpmA and R-GECO; every 2 s, total 180 s. (Scale bar, 2 μm.) See Fig. 3*E*.

Movie S5

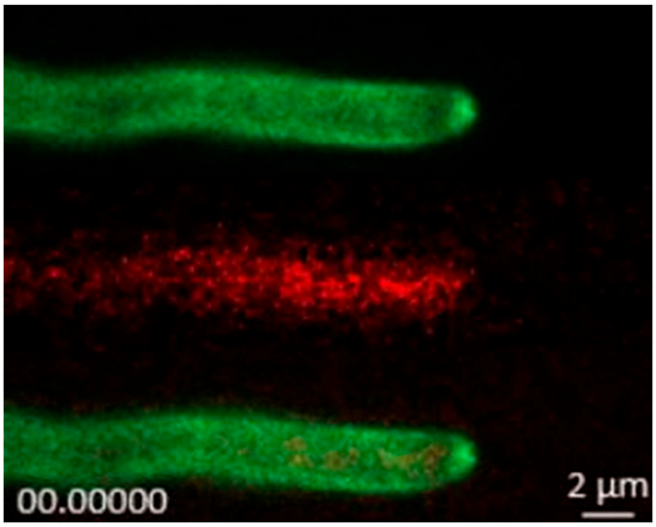

Movie S6. Image sequences of BglA-GFP and R-GECO; every 2 s, total 180 s. (Scale bar, 2 μm.) See Fig. 3*H*.

Movie S6